

STELLAR GRANULATION AS THE SOURCE OF HIGH-FREQUENCY FLICKER IN KEPLER LIGHT CURVES

STEVEN R. CRANMER¹, FABIENNE A. BASTIEN², KEIVAN G. STASSUN^{2,3}, AND STEVEN H. SAAR¹

Draft version June 28, 2021

ABSTRACT

A large fraction of cool, low-mass stars exhibit brightness fluctuations that arise from a combination of convective granulation, acoustic oscillations, magnetic activity, and stellar rotation. Much of the short-timescale variability takes the form of stochastic noise, whose presence may limit the progress of extrasolar planet detection and characterization. In order to lay the groundwork for extracting useful information from these quasi-random signals, we focus on the origin of the granulation-driven component of the variability. We apply existing theoretical scaling relations to predict the star-integrated variability amplitudes for 508 stars with photometric light curves measured by the *Kepler* mission. We also derive an empirical correction factor that aims to account for the suppression of convection in F-dwarf stars with magnetic activity and shallow convection zones. So that we can make predictions of specific observational quantities, we performed Monte Carlo simulations of granulation light curves using a Lorentzian power spectrum. These simulations allowed us to reproduce the so-called “flicker floor” (i.e., a lower bound in the relationship between the full light-curve range and power in short-timescale fluctuations) that was found in the *Kepler* data. The Monte Carlo model also enabled us to convert the modeled fluctuation variance into a flicker amplitude directly comparable with observations. When the magnetic suppression factor described above is applied, the model reproduces the observed correlation between stellar surface gravity and flicker amplitude. Observationally validated models like these provide new and complementary evidence for a possible impact of magnetic activity on the properties of near-surface convection.

Keywords: convection – stars: activity – stars: solar-type – starspots – techniques: photometric

1. INTRODUCTION

The last decade has seen a drastic improvement in the precision of both stellar observations and the consequent determination of accurate fundamental parameters for thousands of nearby stars (e.g., Torres et al. 2010; Chaplin & Miglio 2013). These improvements have also enabled the discovery and characterization of extrasolar planets with a range of sizes that now extends down to less than the radius of the Earth (Barclay et al. 2013). However, Sun-like stars are known to exhibit stochastic variations in both their surface-integrated fluxes (“flicker”) and Doppler radial velocities (“jitter”), and these fluctuations may become a source of noise that limits further progress in planet detection. We aim to improve our understanding of the physical origins of the quasi-random variability associated with stellar activity. This paper focuses on the flicker properties of star-integrated visible continuum light curves; see Saar (2009), Boisse et al. (2011), and Bastien et al. (2013b) for additional studies of radial velocity jitter.

High-resolution observations of the Sun have been important in allowing us to distinguish clearly between a number of distinct signals that appear in stellar light curves. For the Sun, acoustic p -mode oscillations dominate at periods of order 3–5 min. Granulation (i.e., the photospheric signature of the upper boundary of the convective zone) dominates at slightly longer periods extending up to 10–30 min. Sunspot variability—in combination with the evolution of bright plage and facular regions—occurs on timescales of days to months, with a def-

inite peak at the solar rotation period of ~ 27 days. For other stars, the granulation and p -mode timescales are expected to scale with the acoustic cutoff period (e.g., Brown et al. 1991) and most spot-related activity (ignoring impulsive flares associated with magnetic active regions) recurs with the rotation period.

Although stellar p -mode oscillations are increasingly being used for asteroseismic determinations of stellar masses and radii, there has been less work done on extracting useful physics from the granulation signals (see, however, Michel et al. 2008; Ludwig et al. 2009; Kallinger & Matthews 2010; Mathur et al. 2011). In this paper, we follow up on recent observational results from the *Kepler* mission (Borucki et al. 2010) that reported new correlations between the surface gravities of F, G, and K-type stars and the short-timescale flicker properties of their light curves (Bastien et al. 2013a). We make use of theoretical granulation models developed by Samadi et al. (2013a,b) to produce improved predictions of the observed light curve properties as a function of the fundamental stellar parameters. We also show that the empirical correlation between gravity and flicker can be interpreted as a direct signature of granulation.

In Section 2 of this paper, we present the details of the model and we propose an empirical modification to it that accounts for magnetic suppression of granulation in the hottest stars of the sample. Section 3 describes a Monte Carlo model of the granulation light curves that we constructed in order to better understand how the different variability indices of Bastien et al. (2013a) relate to one another and to the intrinsic granulation power. Section 4 summarizes the results, including a reproduction of the surface gravity dependence of the short-time light curve “flicker.” Lastly, Section 5 concludes this paper with a brief summary, a discussion of some of the wider implications of these results, and suggestions for future

¹ Harvard-Smithsonian Center for Astrophysics, 60 Garden Street, Cambridge, MA 02138, USA

² Department of Physics and Astronomy, Vanderbilt University, 1807 Station B, Nashville, TN 37235, USA

³ Physics Department, Fisk University, 1000 17th Avenue North, Nashville, TN 37208, USA

improvements.

2. THE GRANULATION MODEL

2.1. Empirical Scaling Relations

Samadi et al. (2013a,b) presented theoretical scaling relations for how granular fluctuations in a star’s disk-integrated intensity should vary as a function of its fundamental parameters. We apply a slightly modified version of this model below. The root-mean-square amplitude σ of photospheric continuum intensity variations is specified as a function of effective temperature (T_{eff}), surface gravity ($\log g$), and stellar mass (M_*). Samadi et al. (2013b) derived the following scaling,

$$\sigma = 0.039 \left[\left(\frac{T_{\text{eff}}}{T_{\odot}} \right)^{3/4} \left(\frac{M_{\odot} \nu_{\odot}}{M_* \nu_{\text{max}}} \right)^{1/2} \Phi(\mathcal{M}_a)^2 \right]^{1.03} \quad (1)$$

where σ is given in units of parts per thousand (ppt) and Φ is a dimensionless temperature fluctuation amplitude that depends on the turbulent Mach number \mathcal{M}_a (see below). The normalizing constants $T_{\odot} = 5777$ K, $\log g_{\odot} = 4.438$, and $\nu_{\odot} = 3.106$ mHz are taken from Samadi et al. (2013b). The peak frequency ν_{max} of p -mode oscillations is assumed to scale with the acoustic cutoff frequency (e.g., Brown et al. 1991; Kjeldsen & Bedding 1995), with

$$\nu_{\text{max}} = \nu_{\odot} \frac{g}{g_{\odot}} \left(\frac{T_{\odot}}{T_{\text{eff}}} \right)^{1/2}. \quad (2)$$

An additional dependence of ν_{max} on the Mach number \mathcal{M}_a has been proposed (e.g., Belkacem et al. 2011; Belkacem 2012), but we continue to use Equation (2) to retain continuity with other empirical results from asteroseismology.

Equation (1) suggests that σ is nearly linearly proportional to the combined quantity $T_{\text{eff}}^{3/4} M_*^{-1/2} \nu_{\text{max}}^{-1/2}$. This scaling comes from an assumed dependence on the average number of granules \mathcal{N} that are distributed across the visible stellar surface. Ludwig (2006) and Samadi et al. (2013a,b) gave the statistical result that $\sigma \propto \mathcal{N}^{-1/2}$, and \mathcal{N} depends in turn on the stellar radius R_* and the characteristic granule size Λ . Some recent sets of convection models (e.g., Robinson et al. 2004; Magic et al. 2013) show that Λ is close to being linearly proportional to the photospheric scale height $H_* \propto T_{\text{eff}}/g$ over a wide range of stellar parameters. Trampedach et al. (2013) found a slightly modified correlation ($\Lambda \propto T_{\text{eff}}^{1.321} g^{-1.097}$) when modeling convection for both dwarfs and giants, but we retain the usual assumption of $\Lambda \propto H_*$.

Samadi et al. (2013b) also investigated the dependence of the granular intensity contrast on the turbulent Mach number \mathcal{M}_a in a series of three-dimensional simulations of photospheric convection. We use the Samadi et al. (2013b) scaling relation for the Mach number,

$$\mathcal{M}_a = 0.26 \left(\frac{T_{\text{eff}}}{T_{\odot}} \right)^{2.35} \left(\frac{g_{\odot}}{g} \right)^{0.152}, \quad (3)$$

which is then used as input to their parameterized fit for the root-mean square temperature fluctuation amplitude

$$\Phi(\mathcal{M}_a) = -0.67 + 8.85\mathcal{M}_a - 8.73\mathcal{M}_a^2. \quad (4)$$

Note that this fitting formula is strictly applicable only for the range $0.15 < \mathcal{M}_a < 0.45$. The above relations describe an initial, unmodified description of turbulent convection to which we propose a modification in Section 2.2.

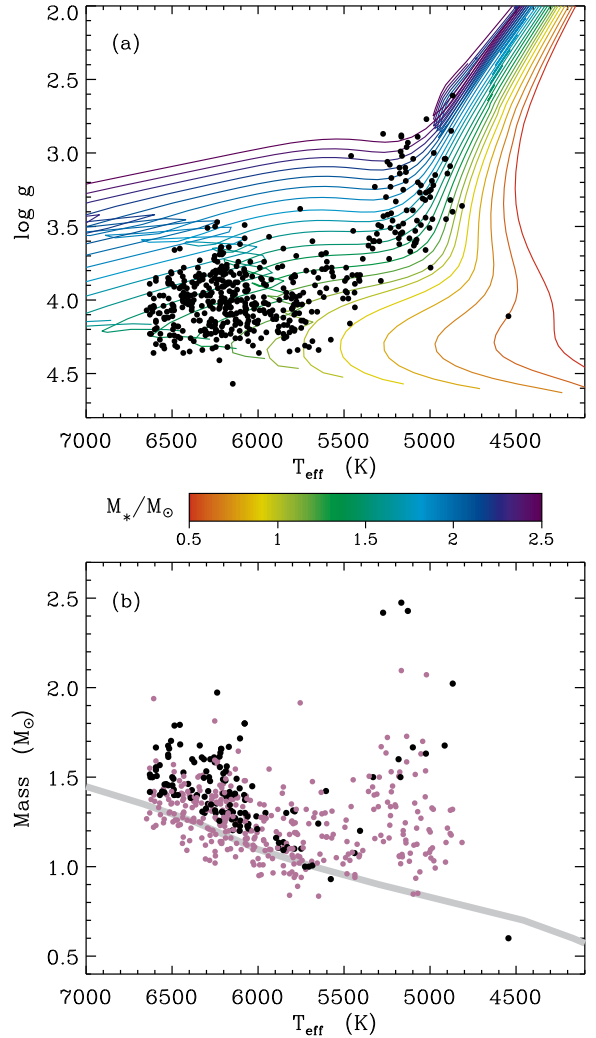


Figure 1. (a) Stellar T_{eff} versus $\log g$ for STARS code evolutionary tracks (solid curves), with masses labeled by different colors, and for the 508 stars studied by Bastien et al. (2013a) (solid circles). (b) Stellar masses from Chaplin et al. (2011b, 2013) (magenta symbols) and masses determined from evolutionary tracks (black symbols), shown alongside an example zero-age main sequence assembled from models of Girardi et al. (2000) and Ekström et al. (2012) (gray curve).

The 508 *Kepler* stars analyzed by Bastien et al. (2013a) all have measured values of T_{eff} and $\log g$ (see Chaplin et al. 2011b; Pinsonneault et al. 2012). However, definitive masses for the full set have not yet been determined. For a subset of 322 of these stars, we used masses computed from recent ensemble asteroseismology (Chaplin et al. 2013). Another 47 of the stars were analyzed in an earlier asteroseismology study (Chaplin et al. 2011b), and we incorporated those masses as well. For the remaining 139 stars, we estimated masses by comparing their measured T_{eff} and $\log g$ values against evolutionary tracks computed by the Cambridge STARS code (Eggleton 1971; Eldridge et al. 2008; Eldridge & Stanway 2009). These single-star models assumed classic solar abundances ($Z = 0.02$) and did not include mass loss. Figure 1(a) compares the tracks to the observationally determined T_{eff} and $\log g$ values of the *Kepler* stars.

Figure 1(b) shows the T_{eff} dependence of the derived stellar masses. Both panels in Figure 1 make it clear that the *Kepler* sample includes a mix of main-sequence dwarfs, mildly evolved subgiants, and more highly evolved red giants. The

masses of Chaplin et al. (2011b) and Chaplin et al. (2013) are shown with magenta symbols. The black symbols show masses that we determined by computing a χ^2 goodness of fit parameter for each $(T_{\text{eff}}, \log g)$ point along the model tracks and weighting the final mass determination by $1/\chi^2$ for all models satisfying $\chi^2 \leq 10 \min(\chi^2)$. We found this to be a less ambiguous process than simple interpolation, since there are places in Figure 1(a) where the tracks cross over one another. This property of the models leads to the existence of multiple local minima in χ^2 space. Thus, we believe that using a weighted average of the low- χ^2 models takes better account of the uncertainties than just selecting the single model point corresponding to the global minimum in χ^2 .

2.2. Magnetic Inhibition of Convection

Although F-type stars tend to exhibit lower levels of chromospheric emission than their cooler G and K counterparts (Isaacson & Fischer 2010), there has been increasing evidence that many of them have strong enough magnetic activity to suppress the amplitudes of atmospheric oscillations and granular variability (Chaplin et al. 2011a; Samadi et al. 2013b). As T_{eff} increases from 6000 to 7000 K and beyond, the convection zone shrinks considerably in thickness. It is suspected that strong-field regions can have a much stronger inhibitive effect on the correspondingly shallower granulation of these stars (e.g., Cattaneo et al. 2003; Moringa et al. 2008). However, the simulations used by Samadi et al. (2013b) did not contain this magnetic suppression effect, and thus Equation (1) was seen to overpredict observed fluctuation amplitudes for the largest values of T_{eff} .

In the absence of a complete theory of magnetic suppression, we decided on an empirical approach to fold in an additional T_{eff} dependence to the turbulent Mach number \mathcal{M}_a . The goal was to leave the predictions of \mathcal{M}_a unmodified for the coolest stars and produce a gradual decrease in the convective velocity field for the hotter, more active stars. We first used Equation (3) to estimate the Mach number for each model, then we multiplied it by a dimensionless suppression factor S given by

$$S = \begin{cases} 1, & T_{\text{eff}} \leq 5400 \text{ K}, \\ 1/[1+(T_{\text{eff}}-5400)/1500], & T_{\text{eff}} > 5400 \text{ K}. \end{cases} \quad (5)$$

As we describe further in Section 4, this form for S was selected in order to produce optimal agreement between the modeled and measured light curve amplitudes for the full range of F, G, and K stars in the *Kepler* sample. Equation (5) is meant to estimate the magnitude of the suppression effect only for stars with $T_{\text{eff}} \lesssim 7000$ K. There may be additional dependencies on other stellar parameters for hotter stars with extremely thin surface convection zones (see also Bercik et al. 2005; Cantiello et al. 2009).

Figure 2 shows the impact of applying the correction factor defined above. Equations (3)–(4) alone would have predicted high values of $\mathcal{M}_a \approx 0.4$ and $\Phi \approx 1.5$ for the hottest stars in the sample. Our correction gives rise to roughly a factor of 1.8 decrease in both \mathcal{M}_a and Φ for the hottest stars. Note that the revised model prediction for the temperature fluctuation amplitude produces values that fall closer to the simple approximation of $\Phi = 1$ that was assumed in earlier studies (Kjeldsen & Bedding 2011; Mathur et al. 2011).

Equations (1)–(5) allow us to compute the root-mean-square amplitude σ for each star in the sample, and for each point along the theoretical evolutionary tracks. However,

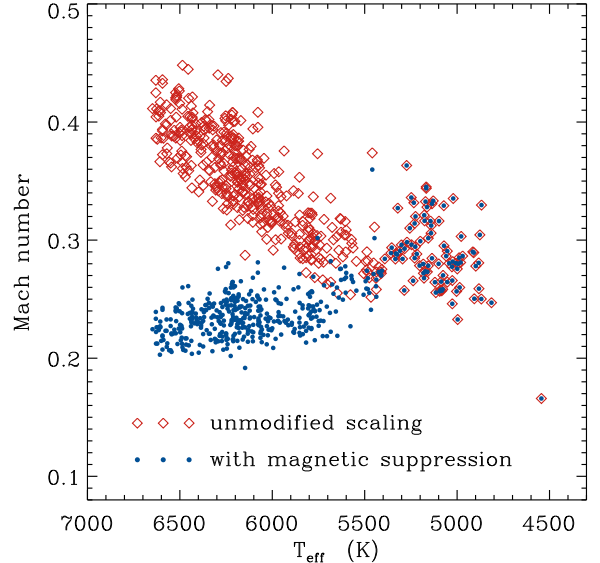


Figure 2. Two estimates for the dimensionless convective Mach number \mathcal{M}_a , shown versus T_{eff} for the 508 *Kepler* stars. Red open diamonds show the result of Equation (3) without modification, and blue filled circles show the result of applying the suppression factor given in Equation (5).

σ does not correspond exactly to observational parameters that are derivable easily from the *Kepler* data.⁴ Following Basri et al. (2011), Bastien et al. (2013a) characterized the light curves with three independent measures of variability:

1. a short-timescale *flicker* amplitude (F_8) that corresponds to fluctuations on timescales of 8 hours or less,
2. the light-curve *range* (R_{var}), defined as the difference between the 5% and 95% percentile intensities, and
3. the number of *zero crossings* (Z_C) experienced by the light curve, smoothed with a 10-hour window, over the full 90 days of the data set.

In this paper we attempt to faithfully reproduce these quantities as they were defined by Basri et al. (2011) and Bastien et al. (2013a). However, computing these parameters from the granulation model requires additional information about the expected frequency spectrum, which we discuss in the following section.

3. STATISTICS OF SIMULATED LIGHT CURVES

In order to better understand how the various measures of photometric variability relate to one another, we constructed Monte Carlo models of light curves for a range of representative stellar parameters. We used a Lorentzian form for the granular power spectrum,

$$\mathcal{P}(\nu) = \frac{4\tau_{\text{eff}}\sigma^2}{1+(2\pi\tau_{\text{eff}}\nu)^2} \quad (6)$$

(e.g., Harvey 1985), where τ_{eff} is a characteristic granulation timescale. The integral of \mathcal{P} over all frequencies ν gives the fluctuation variance σ^2 . However, for these models, we set

⁴ Although it is possible to compute the full frequency spectrum from an observed light curve, and process that spectrum to estimate the values of σ and several other granulation properties (e.g., Michel et al. 2008; Mathur et al. 2011), this procedure is much less straightforward than the light curve metrics discussed here.

$\sigma = 1$ in order to focus on the time-domain structure of the light curves.

The granulation timescales to use in the Monte Carlo models were obtained by first estimating τ_{eff} for each of the observed stars using the scaling relation given by Samadi et al. (2013b),

$$\tau_{\text{eff}} = 300 \left(\frac{\nu_{\odot} \mathcal{M}_{a\odot}}{\nu_{\text{max}} \mathcal{M}_a} \right)^{0.98} \text{ s}, \quad (7)$$

where $\mathcal{M}_{a\odot} = 0.26$. We used the modified version of \mathcal{M}_a described in Section 2.2 as the input quantity to Equation (7). Thus, the estimated values of τ_{eff} for the *Kepler* stars ranged between 300 and 14,000 s, with a median value of 990 s. We then created a set of 500 model light curves with a grid of τ_{eff} values spread out between 150 and 20,000 s, slightly wider than the observed range. Each Monte Carlo light curve was built up from 500 independent frequency components, where the dimensionless frequency $2\pi\tau_{\text{eff}}\nu$ ranged from 0.1 to 100.1 in constant steps of 0.2. Each component was assumed to be a sinusoid with a random phase and a relative amplitude consistent with $\mathcal{P}(\nu)$.

For each set of random Monte Carlo variables, we constructed a full-resolution light curve with a maximum duration of 90 days (one *Kepler* quarter) and a point-to-point time step of 2.5 s. A corresponding “observational” light curve was sampled from it with a spacing of 30 min—as in the *Kepler* low-cadence data—and it was processed in an identical way as the actual data to obtain F_8 , R_{var} , and Z_C . As an example, Figure 3(a) shows a full resolution model light curve, its reduced *Kepler* sampling, and the 8 hr smoothing performed to compute F_8 . For this model, $\tau_{\text{eff}} = 1000$ s, and only a one-day subset of the light curve is shown.

Figure 3(b) shows the ratio F_8/σ as a function of τ_{eff} for the 500 models. For the shortest granular timescales (i.e., $\tau_{\text{eff}} \lesssim 1000$ s), the F_8 diagnostic seems to capture the full granular fluctuation amplitude, and $F_8 \approx \sigma$. Figure 3(b) shows a roughly 10% random scatter around the mean ratio $F_8/\sigma = 1$. We believe this arises from both the random nature of the Monte Carlo models and the 30-min cadence sampling used to obtain the flicker amplitude F_8 . When the 30-min cadence was replaced by a 10-min cadence, the spread in F_8/σ (which we measured by computing the range between the 5% and 95% percentile values of the ratio, for $\tau_{\text{eff}} < 1000$ s) is reduced from 9.7% to 6.7%. It may be the case that this scatter contributes to the root mean square deviation of ~ 0.1 dex that characterizes the spread in the observed correlation between F_8 and $\log g$ (Bastien et al. 2013a).

For the largest values of τ_{eff} , a significant portion of the low-frequency end of the spectrum is excluded by the 8-hr filtering used to compute F_8 . Thus, the ratio F_8/σ is reduced to values as low as ~ 0.5 at the largest value of $\tau_{\text{eff}} = 20,000$ s. We can estimate the quantitative impact of the 8-hr filtering by integrating over the power spectrum (Equation (6)) only for frequencies exceeding $\nu_8 = (8 \text{ hr})^{-1}$. The result, expressed as a ratio of the relevant root-mean-square amplitudes, is

$$\frac{F_8}{\sigma} = \sqrt{1 - \frac{2}{\pi} \tan^{-1}(4\tau_{\text{eff}}\nu_8)}. \quad (8)$$

This expression reproduces the Monte Carlo results shown in Figure 3(b), and we will use it when converting from σ to F_8 below.

We also computed the amplitude ratio R_{var}/F_8 and the all-ready dimensionless number Z_C from the Monte Carlo light

curves. Bastien et al. (2013a) noted that the stars that seemed to be least contaminated by rotating spot activity tend to have the lowest values of R_{var} . Specifically, when R_{var} is plotted as a function of F_8 , there is a noticeably sharp “flicker floor” below which no stars seem to appear. Stars above the floor were interpreted as spot dominated while those on the floor were interpreted as granulation dominated. This floor is described approximately by $R_{\text{var}} \approx 3F_8$. Bastien et al. (2013a) also noted that stars on the flicker floor tend to have the largest values of Z_C , a “zero-crossing ceiling.”

Figure 3(c) compares the modeled R_{var}/F_8 ratios to the observational data. Indeed, the modeled ratio sits very near the observed flicker floor value of 3. The model ratio also increases slightly for the largest values of τ_{eff} , and the observed cool, low-gravity giants in the sample follow this increase as well. In the Monte Carlo models, the ratio R_{var}/σ remains roughly constant no matter the value of τ_{eff} , so the increase in R_{var}/F_8 occurs solely because of the decrease in F_8/σ as shown in Figure 3(b).

It is possible to derive an analytic estimate of R_{var}/F_8 in the small- τ_{eff} limit. For short-timescale granular fluctuations, we showed that F_8 is equivalent to the standard deviation σ of the distribution of intensities that appear in the light curve. The 30 min cadence observations draw effectively random samples from this distribution. If we assume a normal distribution, then the 5% percentile is known to be a value that is 1.6449σ below than mean, and the 95% percentile is 1.6449σ above the mean. Thus, under these assumptions, $R_{\text{var}}/F_8 = 3.2898$. For $\tau_{\text{eff}} \leq 500$ s, Figure 3(c) shows that the modeled R_{var}/F_8 values are given roughly by 3.34 ± 0.16 , which overlaps with the analytic prediction.

Figure 3(d) shows how the Monte Carlo model also seems to reproduce the ceiling in the observed values of Z_C from the *Kepler* sample. As predicted by Bastien et al. (2013a), stars with light curves dominated by granulation exhibit the largest number of zero crossings. Stars with large spots are expected to have light curves dominated by rotational modulation, which produces substantially lower frequency variability than does granulation. For the dwarf stars (i.e., the shortest τ_{eff} timescales), the Monte Carlo models slightly overestimate the upper range of observed values of Z_C . The cool giants, with $\tau_{\text{eff}} \gtrsim 2000$ s, appear to match the model predictions quite well. The stars that fall along the Z_C ceiling are presumably (largely) unspotted and therefore granulation dominated.

A simple prediction for the maximum possible number of zero crossings expected from a noisy, but smoothed, data set would be to assume that $Z_C \approx N/M$, where N is the total number of data points and M is the width of the boxcar averaging window used to smooth the data. For the simulated *Kepler* data, $N = 4320$ (corresponding to 90 days with 30-minute cadence) and $M = 20$ (corresponding to a 10 hr window), and thus $N/M = 216$. However, both the observations and simulations exhibit some data points with Z_C greater than this value.⁵ To refine this prediction, we performed a set of separate simulations using a time series of uniformly distributed random numbers between 0 and 1. We smoothed them, subtracted their median values, and counted up the zero crossings in a similar way as was done with the data. We varied both N and M in order to determine a robust scaling relation for Z_C . These

⁵ Observed or simulated values of Z_C less than this value are easier to understand, since that merely implies a smoother light curve than one that would vary up and down through the median value after every measurement.

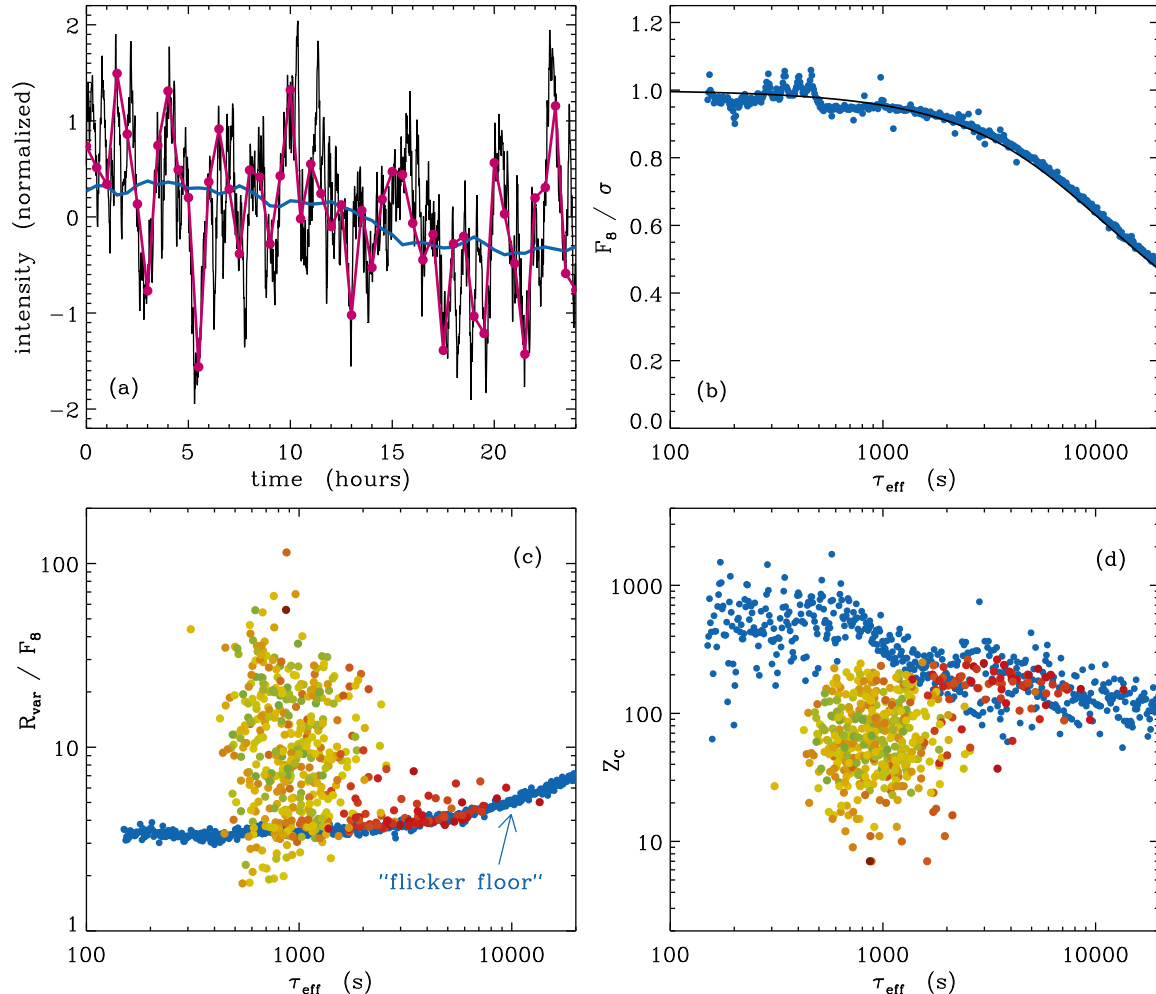


Figure 3. (a) Example Monte Carlo light curve, shown at full resolution (thin black curve) and 30 min *Kepler* resolution (thick magenta curve), along with the 8 hr smoothed version of the *Kepler* light curve that removes nearly all of the granular variability (blue curve). (b) F_8/σ plotted versus τ_{eff} for the 500 Monte Carlo models (blue points) and as given by Equation (8) (black curve). (c) R_{var}/F_8 versus τ_{eff} for the 508 observed stars (with color corresponding to T_{eff} using the scale given in Figure 4) and for the Monte Carlo models (blue points). (d) Same as (c), but for Z_C .

simulations indicated a mean dependence given roughly by

$$Z_C \approx \frac{N}{\sqrt{4M}} \quad (9)$$

which for the *Kepler* data parameters would imply an expectation of $Z_C \approx 480$. For these parameters, the simulations also showed an approximate factor of two spread around the mean value. This is in rough agreement with the simulated light curves shown in Figure 3(d), which for $\tau_{\text{eff}} < 1000$ s have a mean value of $Z_C = 540$. However, the observed sample of dwarf stars in this part of the diagram exhibits a maximum Z_C that is about half of that predicted by the Monte Carlo simulations. This could imply that even the dwarfs with the lowest magnetic activity still possess some low-level starspot or plage coverage that reduces Z_C via rotational modulation.

4. FLICKER VERSUS STELLAR GRAVITY

Lastly, we can use the results of the light curve simulations above to compute model predictions of the flicker amplitude F_8 for the 508 *Kepler* stars. We used Equations (1)–(5) to compute σ and Equation (7) to compute τ_{eff} , then we applied Equation (8) to correct for filtering to obtain F_8 . Figure 4 compares the $\log g$ dependence of the observed flicker parameters to those we computed based on the above model. Without in-

cluding the magnetic suppression effect described in Section 2.2, Figure 4(b) shows that the flicker amplitudes for stars having $T_{\text{eff}} \gtrsim 5700$ K are distinctly larger than observed. We applied the suppression effect, as specified in Equation (5), to produce the agreement between the models and the observations as shown in Figure 4(c).

The arrangement of colors in the lower-left part of Figure 4(c) also suggests there may be a detectable correlation between the flicker amplitude and T_{eff} , with hotter stars experiencing lower absolute fluctuation levels. To explore that idea in more detail, Figure 5 displays how σ depends separately on $\log g$ and T_{eff} for the STARS code evolutionary tracks that were shown in Figure 1. The computed values of σ for the *Kepler* stars are also shown in both panels of Figure 5 as symbols. In addition to the tight $\log g$ dependence that is also seen in Figure 4, there is a slight correlation between σ and T_{eff} . However, Figure 5(b) shows that this apparent T_{eff} dependence is likely to be the result of the age spread of the 508 *Kepler* stars, and the fact that these stars fall along only a relatively narrow set of the evolutionary tracks. As stars with $M_* \approx 1$ – $2 M_\odot$ evolve from high to low $\log g$ and from high to low T_{eff} , they evolve to higher values of σ . Thus, the correlation between σ and T_{eff} may disappear for a more heterogeneous set of observed stars with a broader range of masses.

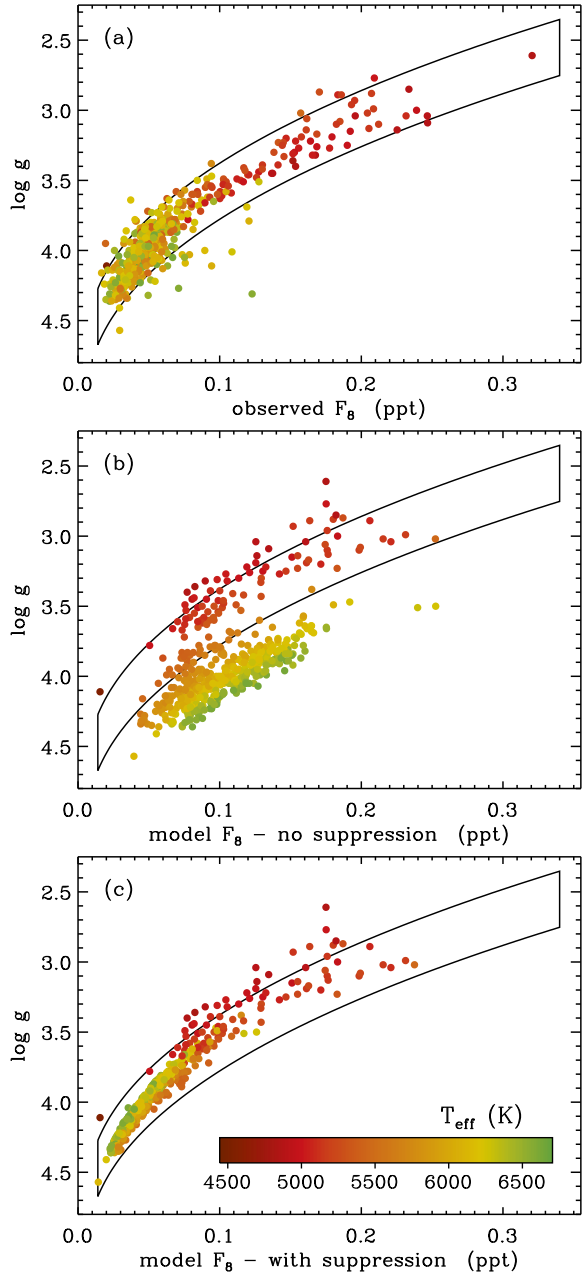


Figure 4. Stellar surface gravity dependence of the light curve flicker amplitude for the *Kepler* sample of 508 stars. (a) Measured values of F_8 from Bastien et al. (2013a). (b) Modeled F_8 computed without magnetic suppression (i.e., $S = 1$). (c) Modeled F_8 computed with Equation (5) for S . Symbol color corresponds to T_{eff} , and the black solid outline shows the polynomial fit given by Bastien et al. (2013a) shifted up and down by factors of ± 0.2 in $\log g$.

Along the zero-age main sequence, the dependence of σ on T_{eff} shown in Figure 5(b) can be fit with an approximate lower-limit amplitude of

$$\sigma_{\text{min}} \approx \frac{0.01x^{14}}{\sqrt{1+x^{23}}}, \quad (10)$$

where $x = T_{\text{eff}}/5000$ K, and we show this relation in Figure 5(b) with a dashed curve. We predict very low intensity fluctuations for the coolest main sequence dwarfs with $\log g > 4.5$ and $T_{\text{eff}} < 4500$ K. For these stars, $\sigma \sim 0.001$ ppt, which would require extremely precise photometry to mea-

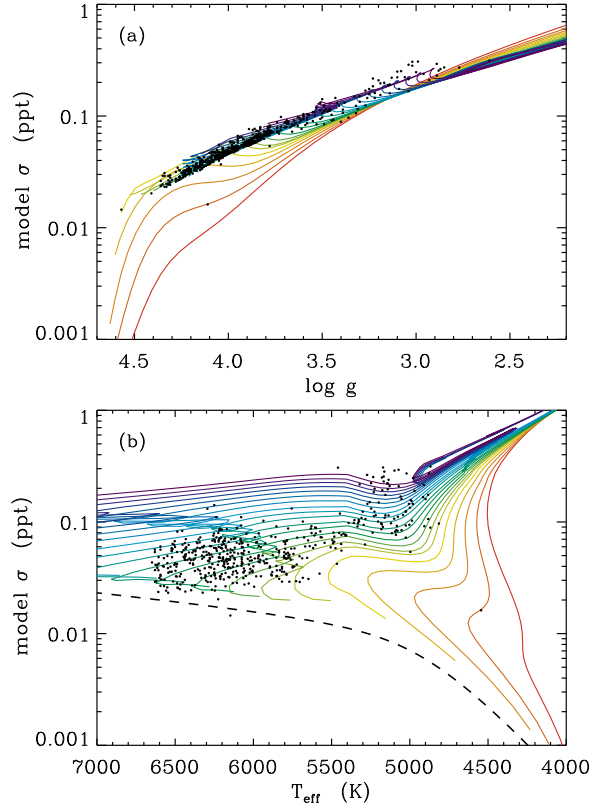


Figure 5. Modeled amplitude σ shown versus (a) $\log g$ and (b) T_{eff} for the STARS evolutionary tracks. See Figure 1 for the color scale that labels each track by M_* . Solid black symbols show the computed σ values for the 508 *Kepler* stars, and the dashed curve is described by Equation (10).

sure. However, these cool dwarfs are also expected to exhibit shorter τ_{eff} timescales that could make the flicker signal more easily measurable.

5. DISCUSSION AND CONCLUSIONS

The goal of this paper was to apply a model of cool-star granulation to the photometric variability of a sample of stars studied by Bastien et al. (2013a). An existing model of granular intensity fluctuations was supplemented by including an ad hoc, but observationally motivated, correction factor for the magnetic suppression of convection in the hottest stars. We also showed how a theoretical frequency spectrum of granular light curve variability could be used to predict some of the other properties of the flicker, range, and zero-crossing diagnostics that were used to analyze the *Kepler* data. The correlation found by Bastien et al. (2013a) between surface gravity and the flicker amplitude was reproduced with the empirically derived magnetic suppression factor. The overall ability of this model to reproduce several different aspects of the observed light curve variability provides evidence that short-timescale intensity fluctuations are a good probe of stellar granulation.

A subsequent goal of this work is to find self-consistent and accurate ways to predict the properties of stellar light curve variability, and to use this variability to calibrate against other methods of determining their fundamental parameters. Thus, it may be possible to develop the analysis of granular flicker measurements in a way that augments the results of asteroseismology and improves the accuracy of, e.g., stellar mass and radius measurements. To assist in this process, we provide tabulated data for the 508 *Kepler* stars analyzed above,

which also includes their derived masses and predicted values of \mathcal{M}_a , σ , and F_8 . These data are given as online-only supplemental material and are hosted, with updates as needed, on the first author's Web site.⁶ Packaged with the data is a short code written in the Interactive Data Language (IDL)⁷ that reads the data and reproduces two of the three panels of Figure 4.

In order to make progress in understanding the properties of granulation light curves, the models need to be improved in several key ways. The scaling relations of Samadi et al. (2013a,b) did not include the effects of varying atmospheric metallicity on σ . Magic et al. (2013) presented a grid of three-dimensional granulation models that were constructed over a range of [Fe/H] values from -4 to $+0.5$ (see also Ludwig et al. 2009; Tremblay et al. 2013). Metallicity appears to have a significant effect on the simulation-averaged granulation intensity contrast, but there is no systematic trend (i.e., in some models, the intensity contrast goes up with increasing [Fe/H], and in others it goes down). It would also be useful to combine the granulation model with accompanying predictions of starspot rotational modulation (e.g., Lanza 2012) and some types of g -mode pulsations that can resemble spot variability (Balona et al. 2011). This could lead the way to predicting the full range of flicker, range, and zero-crossing parameters for the more active stars above the flicker floor.

Another source of uncertainty in the models is that our simple treatment of the magnetic suppression of granulation was assumed to depend only on T_{eff} . It is clearly desirable to move beyond the empirically guided (i.e., ad hoc) correction factor $S(T_{\text{eff}})$ that we derived, but no definite scalings with other stellar properties have emerged. If strong magnetic fields are really at the root of the velocity suppression, then for stars with $T_{\text{eff}} \lesssim 6500$ K (Böhm-Vitense et al. 2002) there should be an additional correlation between velocity suppression and the rotation rate P_{rot}^{-1} , in parallel with well-known relationships between rotation and high-energy activity (e.g., Pizzolato et al. 2003) and rotation and magnetic flux (e.g., Reiners 2012). A correlation between rotation and the suppression effect, if found, might explain the added scatter in F_8 seen for the higher gravity stars (Figure 4(a)). Nevertheless, simulations of the interaction between convection and inhomogeneous magnetic “spots” show that the power in both granular motions and acoustic p -mode oscillations is reduced substantially when the spot coverage grows larger (Mullan 1973; Cattaneo et al. 2003; Parchevsky & Kosovichev 2007; Morinaga et al. 2008). Activity-related changes in the convective Mach number may also affect asteroseismic determinations of quantities like the peak oscillation frequency (Belkacem et al. 2011; Belkacem 2012). Better models of this interaction may be crucial to improving predictions of the inflated radii of M dwarfs (e.g., MacDonald & Mullan 2013; Feiden & Chaboyer 2013), and also to understanding how spots are formed within turbulent convection zones in the first place (Brandenburg et al. 2013).

This paper includes data collected by the *Kepler* mission. Funding for *Kepler* is provided by the NASA Science Mission directorate. The authors gratefully acknowledge William Chaplin and John Eldridge for making their data available for

use in this study. FAB acknowledges support from a NASA Harriet Jenkins graduate fellowship. KGS and FAB acknowledge NSF AST-1009810 and NSF PAARE AST-0849736.

REFERENCES

- Balona, L. A., Guzik, J. A., Uytterhoeven, K., et al. 2011, *MNRAS*, 415, 3531
- Barclay, T., Rowe, J. F., Lissauer, J. J., et al. 2013, *Nature*, 494, 452
- Basri, G., Walkowicz, L. M., Batalha, N., et al. 2011, *AJ*, 141, 20
- Bastien, F. A., Stassun, K. G., Basri, G., et al. 2013a, *Nature*, 500, 427
- Bastien, F. A., Stassun, K. G., Pepper, J., et al. 2013b, *ApJ*, in press, arXiv:1310.7152
- Belkacem, K., in SF2A-2012: Proc. Ann. Meeting of the French Soc. Astron. Astrophys., ed. S. Boissier, P. de Laverny, N. Nardetto, R. Samadi, D. Valls-Gabaud, H. Wozniak, 173
- Belkacem, K., Goupil, M. J., Dupret, M. A., et al. 2011, *A&A*, 530, A142
- Bercik, D. J., Fisher, G. H., Johns-Krull, C. M., & Abbett, W. P. 2005, *ApJ*, 631, 529
- Böhm-Vitense, E., Robinson, R., Carpenter, K., et al. 2002, *ApJ*, 569, 941
- Boisse, I., Bouchy, F., Hébrard, G., et al. 2011, *A&A*, 528, A4
- Borucki, W. J., Koch, D., Basri, G., et al. 2010, *Science*, 327, 977
- Brandenburg, A., Kleeorin, N., & Rogachevskii, I. 2013, *ApJ*, 776, L23
- Brown, T. M., Gilliland, R. L., Noyes, R. W., & Ramsey, L. W. 1991, *ApJ*, 368, 599
- Cantiello, M., Langer, N., Brott, I., et al. 2009, *A&A*, 499, 279
- Cattaneo, F., Emonet, T., & Weiss, N. 2003, *ApJ*, 588, 1183
- Chaplin, W. J., Basu, S., Huber, D., et al. 2013, *ApJS*, in press, arXiv:1310.4001
- Chaplin, W. J., Bedding, T. R., Bonanno, A., et al. 2011a, *ApJ*, 732, L5
- Chaplin, W. J., Kjeldsen, H., Christensen-Dalsgaard, J. 2011b, *Science*, 332, 213
- Chaplin, W. J., & Miglio, A. 2013, *ARA&A*, 51, 353
- Eggleton, P. P. 1971, *MNRAS*, 151, 351
- Ekström, S., Georgy, C., Eggenberger, P., et al. 2012, *A&A*, 537, A146
- Eldridge, J. J., Izzard, R. G., & Tout, C. A. 2008, *MNRAS*, 384, 1109
- Eldridge, J. J., & Stanway, E. R. 2009, *MNRAS*, 400, 1019
- Feiden, G. A., & Chaboyer, B. 2013, *ApJ*, submitted, arXiv:1309.0033
- Girardi, L., Bressan, A., Bertelli, G., & Chiosi, C. 2000, *A&AS*, 141, 371
- Harvey, J. 1985, in *Future Missions in Solar, Heliospheric and Space Plasma Physics*, ed. E. Rolfe & B. Battrock (ESA-SP 235; Noordwijk: ESA), 199
- Isaacson, H., & Fischer, D. 2010, *ApJ*, 725, 875
- Kallinger, T., & Matthews, J. M. 2010, *ApJ*, 711, L35
- Kjeldsen, H., & Bedding, T. R. 1995, *A&A*, 293, 87
- Kjeldsen, H., & Bedding, T. R. 2011, *A&A*, 529, L8
- Lanza, A. F. 2012, in *Astrophys. Space Sci. Proc. 31, Stellar Pulsations*, ed. L. Balona, J. Christensen-Dalsgaard, R. Garrido, J. Suarez (Berlin: Springer), 215
- Ludwig, H.-G. 2006, *A&A*, 445, 661
- Ludwig, H.-G., Samadi, R., Steffen, M., et al. 2009, *A&A*, 506, 167
- MacDonald, J., & Mullan, D. J. 2013, *ApJ*, 765, 126
- Magic, Z., Collet, R., Asplund, M., et al. 2013, *A&A*, 557, A26
- Mathur, S., Hekker, S., Trampedach, R., et al. 2011, *ApJ*, 741, 119
- Michel, E., Baglin, A., Auvergne, M., et al. 2008, *Science*, 322, 558
- Morinaga, S., Sakurai, T., Ichimoto, K., et al. 2008, *A&A*, 481, L29
- Mullan, D. J. 1973, *Irish Astron. J.*, 11, 32
- Parchevsky, K. V., & Kosovichev, A. G. 2007, *ApJ*, 666, 547
- Pinsonneault, M. H., An, D., Molenda-Zakowicz, J., et al. 2012, *ApJS*, 199, 30
- Pizzolato, N., Maggio, A., Micela, G., et al. 2003, *A&A*, 397, 147
- Reiners, A. 2012, *Living Rev. Solar Phys.*, 9, 1
- Robinson, F. J., Demarque, P., Li, L. H., et al. 2004, *MNRAS*, 347, 1208
- Saar, S. H. 2009, in *AIP Conf. Proc. 1094, 15th Cambridge Workshop on Cool Stars, Stellar Systems, and the Sun*, 152
- Samadi, R., Belkacem, K., & Ludwig, H.-G. 2013a, *A&A*, 559, A39
- Samadi, R., Belkacem, K., Ludwig, H.-G., et al. 2013b, *A&A*, 559, A40
- Torres, G., Andersen, J., & Giménez, A. 2010, *A&A Rev.*, 18, 67
- Trampedach, R., Asplund, M., Collet, R., et al. 2013, *ApJ*, 769, 18
- Tremblay, P.-E., Ludwig, H.-G., Freytag, B., et al. 2013, *A&A*, 557, A7

⁶ <http://www.cfa.harvard.edu/~scanmer/>

⁷ IDL is published by ITT Visual Information Solutions. There are also several free implementations with compatible syntax, including the GNU

Data Language (GDL) and the Perl Data Language (PDL).